UNIVERSITÄT AUGSBURG
Universitätsbibliothek

OPEN ACCESS
OPUS AUGSBURG

Porous glass-ceramics from alkali activation and sinter-crystallization of mixtures of waste glass and residues from plasma processing of municipal solid waste

Patricia Rabelo Monich, Acacio Rincón Romero, Daniel Höllen, Enrico Bernardo

Angaben zur Veröffentlichung / Publication details:

Rabelo Monich, Patricia, Acacio Rincón Romero, Daniel Höllen, and Enrico Bernardo. 2018. "Porous glass-ceramics from alkali activation and sinter-crystallization of mixtures of waste glass and residues from plasma processing of municipal solid waste." *Journal of Cleaner Production* 188: 871–78. https://doi.org/10.1016/j.jclepro.2018.03.167.

Nutzungsbedingungen / Terms of use: **CC BY-NC-ND 4.0**

Dieses Dokument wird unter folgenden Bedingungen zur Verfügung gestellt: / This document is made available under these conditions:
CC-BY-NC-ND 4.0: Creative Commons: Namensnennung - Nicht kommerziell - Keine Bearbeitung
Weitere Informationen finden Sie unter: / For more information see:
https://creativecommons.org/licenses/by-nc-nd/4.0/deed.de

Journal of Cleaner Production 188 (2018) 871–878

Contents lists available at ScienceDirect

Journal of Cleaner Production

journal homepage: www.elsevier.com/locate/jclepro

Porous glass-ceramics from alkali activation and sinter-crystallization of mixtures of waste glass and residues from plasma processing of municipal solid waste

Patricia Rabelo Monich [a], Acacio Rincón Romero [a], Daniel Höllen [b], Enrico Bernardo [a, *]

[a] Dipartimento di Ingegneria Industriale, Università Degli Studi di Padova, Via Marzolo 9, 35131 Padova, Italy
[b] Chair of Waste Processing Technology and Waste Management, Montanuniversität Leoben, Franz-Josef-Str. 18, 8700 Leoben, Austria

ARTICLE INFO

Article history:
Received 11 December 2017
Received in revised form
27 February 2018
Accepted 16 March 2018
Available online 6 April 2018

Keywords:
Alkali activation
Gel casting
Glass-ceramic foams
Waste glasses
Upcycling

ABSTRACT

Alkali-activated aqueous slurries of fine glass powders, mostly deriving from the plasma processing of municipal solid waste ('Plasmastone'), were found to undergo progressive hardening at low temperature (75 °C) owing to the formation of C–S–H (calcium silicate hydrate) gels. Before complete setting, slurries could be easily foamed by vigorous mechanical stirring, with the help of a surfactant; finally, the resulting open-celled structure could be 'frozen' by a subsequent sintering treatment, with crystallization of Ca–Fe silicates. The densification of the struts upon firing was enhanced by mixing Plasmastone with up to 30 wt% recycled glasses and increasing the firing temperature from 800 to 1000 °C. A total porosity exceeding 75 vol%, comprising both well-interconnected macro- and micro-sized pores on cell walls, was accompanied by good compressive strength, well above 1 MPa. The stabilization of pollutants generally increased with increasing firing temperature and glass content, with some exceptions; no practical leaching was observed from samples deriving from Plasmastone combined with 30 wt% boro-alumino-silicate glass from the recycling of pharmaceutical vials.

© 2018 The Authors. Published by Elsevier Ltd. This is an open access article under the CC BY-NC-ND license (http://creativecommons.org/licenses/by-nc-nd/4.0/).

1. Introduction

Glass foams represent a very interesting class of materials due to high surface area and permeability, low density and specific heat, high thermal and acoustic insulation and high chemical resistance. In addition, unlike polymeric foams, glass foams are non-flammable and flame resistant, chemically inert and not toxic (Rincón et al., 2016). Therefore, cellular glass materials have the potential to replace polymeric foams as building insulation materials, thus aiding in minimizing damages in case of fire.

Compared to polymer foams, glass foams are currently far more expensive, owing to the specific processing. The most established method consists of the mixing of glass powders with a foaming agent, followed by firing. During the heat treatment, glass powders soften and form a 'pyroplastic' mass, foamed as an effect of gas evolution from the additive, in turn depending on decomposition or oxidation reactions. The control of viscous flow sintering and foaming phenomena is quite delicate: as an example, oxygen from the firing atmosphere could not reach C-containing foaming agents, so that further additives ('oxidizers', such as MnO_2 and $CaSO_4$) are needed for optimizing the gas release. In addition, in the case of glass-ceramic foams, the situation is even more delicate, since glass sintering and gas evolution must be combined with crystallization (Rincón et al., 2016).

In an effort to reduce the costs of glass foams processing, a new technique was developed by Rincón et al. (2017). The distinctive character of the new technique is the separation between foaming and sintering. The approach, applied to soda-lime glass, combined alkali activation and firing. More specifically, suspensions of fine glass powders in alkaline aqueous solutions exhibited a marked pseudoplasticity, according to partial dissolution of glass and gelification of the corrosion products. Air bubbles, incorporated by intensive mechanical stirring (with the help of surfactants), at high shear rates and low viscosity, remained 'frozen' when stirring stopped, at low shear rate and high viscosity, configuring an 'inorganic gel casting'. A cellular structure was thus available at low temperature, in samples in 'green' state. Firing treatments were applied after a drying step, at only 700 °C, instead of 850–1000 °C (necessary for the usual foaming reactions to occur), used for conventional glass foams.

* Corresponding author.
E-mail address: enrico.bernardo@unipd.it (E. Bernardo).

https://doi.org/10.1016/j.jclepro.2018.03.167
0959-6526/© 2018 The Authors. Published by Elsevier Ltd. This is an open access article under the CC BY-NC-ND license (http://creativecommons.org/licenses/by-nc-nd/4.0/).

The low temperature foaming, after alkali activation, was conceptually close to that of geopolymer foams (Strozi Cilla et al., 2014). However, it must be noted that the activation was much weaker and the nature of the developed gels was completely different. While in true geopolymers the hardening is associated to the formation of a three-dimensional network structure, from the polymerization of smaller units (in turn provided by the complete dissolution of alumino-silicate raw materials), glass suspensions were stabilized by the formation and interlocking of calcium silicate hydrates (C–S–H) at the surface of powders (Cyr et al., 2012; Garcia-Lodeiro et al., 2016; Rincón et al., 2017).

C–S–H are well known products of alkaline attack, in general, of any CaO-rich silicate glass. As a consequence, the successful extension of the approach, from soda-lime glass, to Ca–Mg silicate bioglass, was not surprising (Elsayed et al., 2017). Interestingly, the open-celled structure available after low temperature foaming, in this case, was maintained with the precipitation of Ca and Ca–Mg silicate crystals (wollastonite and diopside), impeding significant viscous flow upon firing.

The present paper aims at further extending the approach to inorganic residues from municipal solid waste (MSW). Plasma heating has distinctive advantages in resource recovery from waste, since it provides both gasification of organics, by pyrolysis, and metal separation upon melting (owing to reducing conditions) (Scanarc, 2017). This approach is not attractive only with respect to the treatment of fresh MSW, but also with respect to the treatment of excavated MSW, which has been disposed of during the last decades ("Landfill Mining", LFM). Material recovery from LFM is limited to metals which are present only in amounts of 3–5 wt% (Krook et al., 2012; Wolfsberger et al., 2015b). Consequently, energy recovery is the key technology in LFM projects. However, co-incineration in cement kilns is limited by high concentrations of heavy metals (Wolfsberger et al., 2015a).

Incineration using grate furnace technology represents the state of the art for energy recovery of MSW and fractions thereof, which do not fulfil the requirements for co-incineration. However, this yields to the formation of large amounts of bottom ashes, which are even higher for landfilled MSW than for fresh MSW, considering the degradation of organics and the relative enrichment of the mineral fraction in the landfill. Re-landfilling of bottom ashes, due to the high total and leachable contents of heavy metals, is recommended (e.g. in Austria, according to Federal Waste Management Plan Austria 2017).

Plasma gasification is an alternative technology to avoid re-landfilling charges and to recover energy from waste-derived gas ('Syngas') as well as metals. A true 'zero waste' condition and enhanced economical sustainability, however, rely on the obtainment of added value products from the vitreous by-product of the plasma heating process ('Plasmastone') (Jones et al., 2013; Machiels et al., 2016).

Compared to bottom ash produced from the same MSW plasmastone is characterized by lower contents of volatile heavy metals (Pb, Zn), due to higher temperatures, but also of Cu and Ni which can be directed to the metallic phase when reducing conditions are applied (Machiels et al., 2016). The simple use of Plasmastone as building material does not justify the increased effort for plasma gasification compared to incineration (Winterstetter et al., 2015). Therefore, the production of inorganic polymers, i.e. the complete dissolution of Plasmastone in much stronger alkaline solutions, followed by gelification, was suggested for Plasmastone beneficiation. In this study we present an alternative route, consisting of the production of highly porous glass ceramics. The remarkable content of iron oxide is interesting, for the possible phase separation upon firing, in turn bringing new functionalities (e.g. ferrimagnetism) (Ponsot et al., 2014). The mixing with recycled glasses, such as soda-lime glass and boro-alumino-silicate glass from disposed pharmaceutical vials, is discussed as a fundamental tool for improving the sintering and the chemical stability of the developed foams.

2. Experimental procedure

Plasmastone (PS) was gently provided by Scanarc (Sweden) (Scanarc, 2017). The chemical composition of this residue (determined by X-Ray fluorescence) is reported in Table 1. Received in form of granules with a mean particle size of 10 m, it was ground into fine powders, below 75 μm, by dry ball milling. Soda-lime glass (SLG) powders (medium particle size equal to 30 μm) were gently provided by SASIL SpA (Brusnengo, Biella, Italy), as the fraction obtained from glass cullet after colour selection and removal of metallic and polymeric residues (essentially not employed due to the presence of ceramic contaminations) (Rincón et al., 2017). Boro-alumino-silicate glass (BSG), from disposed pharmaceutical vials, was finally provided by Nuova OMPI (Piombino Dese, Padova, Italy); received in form of coarse fragments, it was ground into powders below 45 μm, again by ball milling. The composition of the two recycled glasses is also reported in Table 1 (Ponsot et al., 2014).

Differential thermal analysis (DTA/TGA, STA409, Netzsch Gerätebau GmbH), with heating rate of 10 °C/min) was done on Plasmastone, in form of coarse fragments as well as of fine powders of Plasmastone in order to determine the chemical reactions and physical changes which would occur during a sintering process.

Plasmastone and soda-lime glass (quantities of 0–30 wt%) powders were cast in an alkaline activating solution of 2.5 M NaOH/KOH (ratio 1:1), for an overall solid loading of 68 wt%, under mechanical stirring at 400 rpm. After 3 h of alkaline activation, the suspension was poured in a closed polystyrene mould (60 mm diameter) and cured at 75 °C to undergo gelification (4 h for foams with only Plasmastone, and 3 h for foams from SLG-containing mixtures). Partially gelified suspension were added to 4 wt% Triton X-100 (polyoxyethylene octyl phenyl ether – $C_{14}H_{22}O(C_2H_4O)_n$, n = 9–10, Sigma-Aldrich, Gillingham, UK) surfactant and then subjected to intensive mechanical stirring at 2000 rpm. The resulting 'green' foams were then dried at 40 °C, for 48 h, before being demoulded. Finally, a sintering treatment was applied to stabilize the foams at 800–1000 °C, using a heating rate of 10 °C/min and a holding time of 1 h (Rincón et al., 2017). The produced samples were labelled as XPST, where X is equal to the quantity of Plasmastone used (100 wt%, 90 wt%, 80 wt% or 70 wt%) and T is equal to the temperature employed for sintering (800–1000 °C). 70 wt% Plasmastone/30 wt% boro-alumino-silicate glass foams (30BSG) mixture was subjected to the same treatments, except for a longer curing time at 75 °C (increased up to 6 h) and firing temperature limited to 1000 °C.

The mineralogical analysis of powdered glass-ceramics was

Table 1
Chemical composition of the involved materials (wt%).

	Plasmastone	SLG	BSG
SiO_2	34.26–37.32	71.9	72
TiO_2	0.60–0.67	0.1	
Al_2O_3	12.82–14.79	1.2	7
Fe_2O_3	20.92–24.84	0.3	
MnO	0.11–0.15		
MgO	1.18–2.40	4	
CaO	22.97–23.20	7.5	1
Na_2O	0.26–1.10	14.3	6
K_2O	0.32–0.51	0.4	2
P_2O_5	0.03–0.18		
B_2O_3			12

conducted by means of X-ray diffraction (XRD) (Bruker D8 Advance, Karlsruhe, Germany), using CuKα radiation, 0.15418 nm, 40 kV–40 mA, 2θ = 10–70°, step size 0.05°, 2 s counting time. The phase identification was performed by means of the Match!® program package (Crystal Impact GbR, Bonn, Germany), supported by data from Powder Diffraction File (PDF)-2 database (International Centre for Diffraction Data, Newtown Square, PA, USA).

Fourier-transform infrared spectroscopy (FTIR, FTIR model 2000, Perkin Elmer Waltham, MA) was performed on selected samples to determine their phase composition.

After sintering, the foams were cut into cubes with approximate dimensions of 10 mm × 10 mm × 10 mm. The bulk density of the foams was determined from the weight-to-volume ratio, using a caliper and a digital balance. The apparent and the true densities of the samples were measured by means of a gas pycnometer (Micromeritics AccuPyc 1330, Norcross, GA), operating with He gas on foam block or finely milled samples, respectively. The compressive strength of foams was measured at room temperature, by means of an Instron 1121 UTM (Instron Danvers, MA) operating with a cross-head speed of 1 mm/min. Each data point represents the average value of 5–10 individual tests.

Optical stereomicroscopy (AxioCam ERc 5 s Microscope Camera, Carl Zeiss Microscopy, Thornwood, New York, USA) was employed for the morphological and microstructural characterizations of the porous glass-ceramics.

Leaching tests on foams were performed following ÖNORM EN 12457-4 (Norm EN 12457–4, 2002). A commercial glass foam from Misapor (2017) was used as control. Firstly, the samples (control and produced samples) were crushed into pieces smaller than 10 mm. Then, 10 g of the material was added in a separate bottle containing 100 mL of pure distilled water, in order to obtain a liquid to solid ratio of 10. This suspension was left mixing in an overhead shaker for 24 h. Thereafter, the suspension was poured in a smaller flask and centrifuged in order to separate the solid material from the liquid, thus obtaining the eluate. Inductively coupled plasma mass spectrometry (ICP-MS, Agilent 7500 cx) and ion chromatography (IC, Dionex ICS 2000) were used to measure the contents of heavy metals and anions, respectively, in the leachates and the Austrian Recycling Building Materials Ordinance was used as a reference. For a better understanding of the relation between mineralogy and leachability selected samples were analysed at an electron microprobe (Jeol JXA 8200 Superprobe), after polishing (using 1 μm-sized diamond suspension and diamond spray) and coating with a thin carbon layer.

3. Results and discussion

The DTA analysis (Fig. 1) performed on fine and coarse Plasmastone evidenced that Plasmastone was sensitive to surface crystallization, as the crystallization peak (T_c) of Plasmastone moved towards lower temperatures with decreasing particle size (Rincón et al., 2016). The crystallization peak of the fine powder lied around 800 °C and it was taken as a reference for sintering experiments (performed at T_c and also at T_c+100 °C and T_c+200 °C).

As shown by the FTIR spectra in Fig. 2, Plasmastone exhibited, after activation, a well visible absorption band of hydrated calcium silicate compounds (C–S–H) centred at about 3400 cm^{-1}. This band was even enhanced when considering mixtures with soda-lime glass (also rich in CaO). The band, not visible in the as-received conditions, disappeared after firing above 800 °C. The water release associated with the decomposition of hydrated compounds was thought to contribute to the cellular structure ('secondary foaming'), upon firing. A slight contribution could actually come also from CO_2 release (the formation of carbonates is testified by the peak at 1400 cm^{-1}). The surfactant, visible from peaks attributable to vibrations of C–H bonds (C–H_2 stretch at about 2800 cm^{-1}), did not provide any contribution, upon firing, being completely decomposed below 400 °C (Rincón et al., 2017).

The alkali activation was poorly detectable by X-ray diffraction analysis, as shown by Fig. 3a. We can note only a slight shift of the characteristic 'halo' of glassy materials, as observed with soda-lime glass. The firing treatments, on the contrary, led to substantial changes, with a remarkable crystallization starting at 800 °C. The patterns revealed a quite complex overlapping of contributions from Fe-rich silicates, such as pyroxene (hedenbergite, $Ca(Fe_{0.821}Al_{0.179})(SiAl_{0.822}Fe_{0.178})O_6$, PDF #78–1546) and andradite ($Ca_3Fe_2(SiO_4)_3$, PDF#84–1935. From the same Fig. 3a we can note that the major peaks of iron-rich silicates actually overlapped (see arrows) with those of magnetite (Fe3O4, PDF #89–0691, "M") and hematite (Fe2O3, PDF # 89–2810, "H"). Magnetite cannot be excluded, at least at 800 °C, since the samples exhibited a magnetic behaviour (they were attracted by a permanent magnet). The separation of hematite and magnetite would not be surprising, since it is well known that iron oxides are soluble in molten glass, at high temperature, whereas the solubility decreases at lower temperatures; this justifies the role as nucleating agents, especially for iron-rich pyroxenes (Höland and Beall, 2002; Karamanov et al., 2004b, 2000; Pisciella and Pelino, 2005).

The increase of firing temperature caused an increase of crystallization degree, as testified by the enhanced intensity of diffraction peaks. In addition, a third main phase, consisting of Mg– and Fe-doped bearing gehlenite ($(Ca_{1.96}Na_{.05})(Mg_{.24}Al_{.64}Fe_{.12})(Si_{1.39}Al_{.61}O_7)$, PDF#72–2128), appeared.

Foams from pure Plasmastone were particularly brittle. This was reasonably due to the same intensive crystallization, limiting the viscous flow upon firing. As previously found (Bernardo et al., 2010), the crystallization/flow balance can be adjusted not only 'a priori', by controlling the chemical composition of a glass subjected to sinter-crystallization, but also 'a posteriori', i.e. mixing a glass exhibiting a substantial crystallization with a glass less prone to devitrification, and thus offering simply extra liquid phase upon firing. Fig. 3b shows that this was not completely true, when coupling Plasmastone with soda-lime glass. For samples fired at 1000 °C, it can be seen that the soda-lime glass addition caused a reduction of gehlenite and andradite, but stimulated the precipitation of wollastonite ($CaSiO_3$, PDF #84–0655).

The density and porosity of Plasmastone-derived foams sintered at different temperatures is presented in Table 2. It can be seen that the foams were highly porous, the total porosity being higher than 70 vol%. The porosity was also mostly open, given the close matching between apparent density (ideally referring to the density of the solid still comprising closed cells) and true density (ideally referring to the density of the solid without any pore). The decrease of the porosity from 800 °C to 900 °C was probably due to the increased viscous flow of the residual glass phase. On the other hand, the increase of porosity for foams fired at 1000 °C could be due to secondary foaming phenomena, such as reduction of ferric ions to ferrous ions (in both crystal and amorphous phases), with oxygen evolution (Ponsot et al., 2014).

Table 2 reports also the density data of foams from the addition of recycled glasses. As mentioned above, the addition of soda-lime glass had a poor impact on viscous flow, with the formation of wollastonite. The overall porosity remained at about 80 vol%, mostly open.

The similarity between foams fired at 1000 °C, independently from the soda-lime glass content is confirmed by the microstructures shown in Fig. 4. The brittleness of foams from pure Plasmastone was probably caused by the specific phase assemblage, i.e. it could derive from thermal stresses arising upon cooling between the different phases (Mastelaro and Zanotto, 1996). The addition of

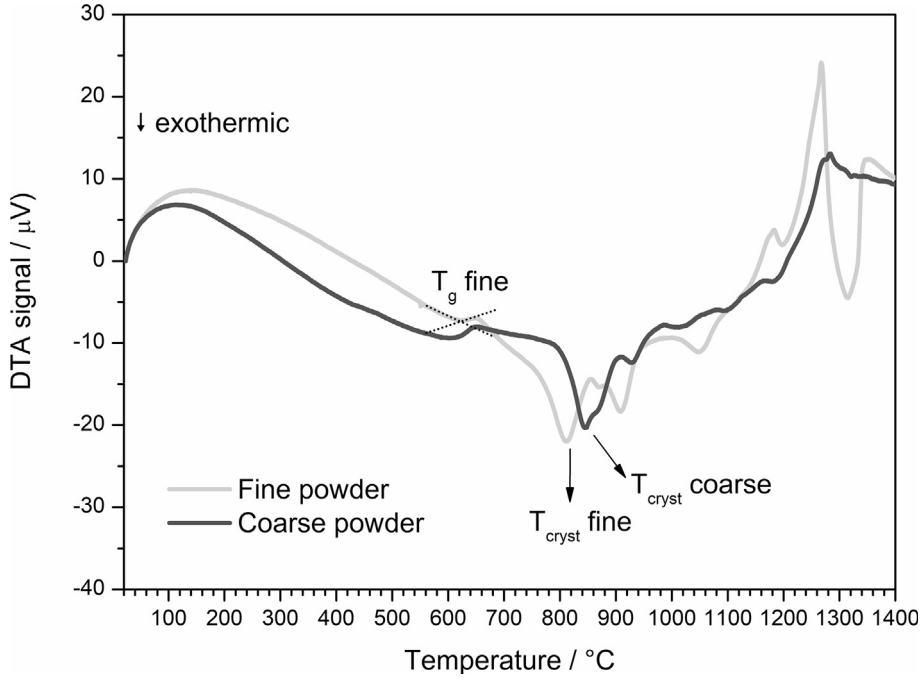

Fig. 1. Differential thermal analysis plots for fine and coarse glass powders of Plasmastone.

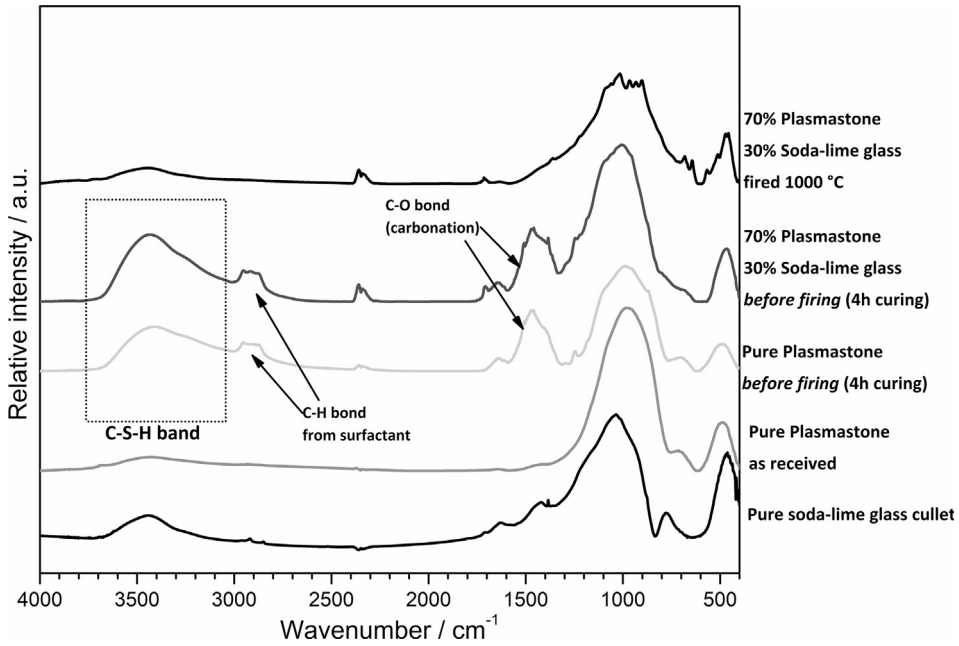

Fig. 2. FTIR spectra of soda-lime glass and Plasmastone derived materials.

soda-lime glass led to significant improvements, as shown by Table 2, by modifying both the typology of crystal phases and the composition of the residual amorphous phase. The table actually reports also the estimated bending strength of the solid phase (σ_{bend}), according to the Gibson-Ashby model (Gibson and Ashby, 1999) for the scaling of compressive strength with relative density:

$$\sigma_{comp} \approx \sigma_{bend}\left[0.2(\phi\rho_{rel})^{3/2} + (1-\phi)\rho_{rel}\right]$$

where the relative density is defined as $\rho_{rel} = 1\text{-}(P/100)$. Owing to the observed limited closed porosity, the shape factor ϕ (amount of solid at the cell edges) was assumed to be equal to 1. The bending strength, for the best foam from soda-lime addition (30SLG1000), is consistent with the strength values of most glasses (Bernardo et al., 2004). This optimized foam could find applications, in buildings, as thermal and acoustic insulators; the proposed gel casting technology is undoubtedly advantageous for the manufacturing of panels (the low temperature foaming does not imply any geometrical limitation). The open-celled morphology and the abundant content of iron oxide could favour additional application, e.g. as catalytic supports.

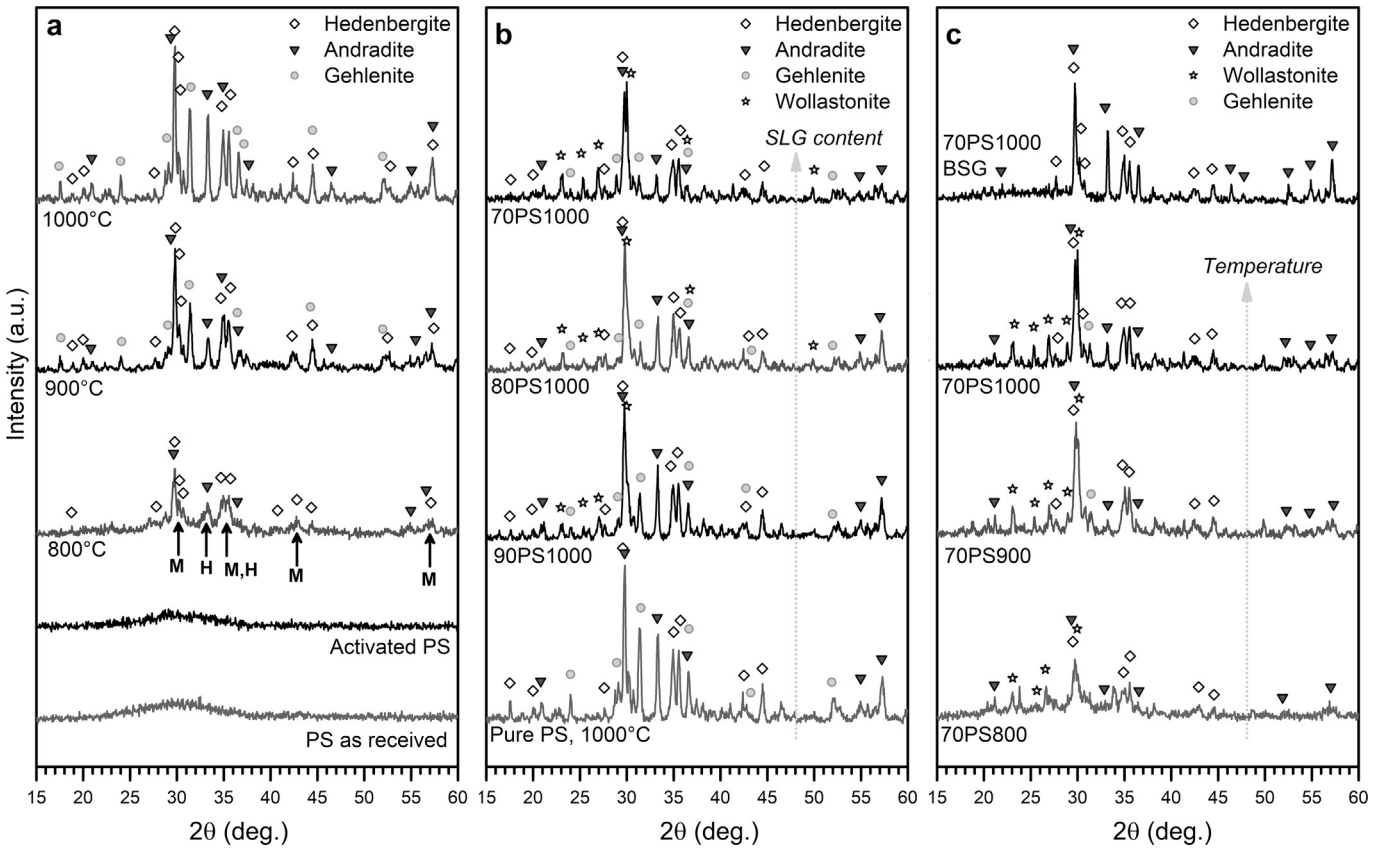

Fig. 3. Phase evolution in glass-ceramic foams: a) pure Plasmastone, after activation and fired at different temperatures; b) Plasmastone mixed with different amounts of SLG, fired at 1000 °C; c) evolution with 30% glass (SLG and BSG).

Table 2
Physical and mechanical properties of selected Plasmastone-based foams.

Formulation	Pure Plasmastone			Plasmastone + Recycled glass			
Glass amount (wt%)	–			10	20	30	30
Glass type	–			SLG			BSG
Firing T (°C)	800	900	1000				
Density determinations							
ρ_{geom} (g/cm^3)	0.81 ± 0.01	0.98 ± 0.02	0.60 ± 0.01	0.67 ± 0.01	0.58 ± 0.03	0.65 ± 0.02	0.78 ± 0.00
$\rho_{apparent}$ (g/cm^3)	2.83 ± 0.06	3.11 ± 0.10	3.32 ± 0.01	3.18 ± 0.03	3.01 ± 0.02	2.92 ± 0.02	2.62 ± 0.04
ρ_{true} (g/cm^3)	3.17 ± 0.01	3.31 ± 0.01	3.32 ± 0.01	3.19 ± 0.01	3.07 ± 0.01	3.20 ± 0.01	3.04 ± 0.01
Porosity distribution							
Total porosity, P (%)	74.4	70.4	81.9	79.1	81.2	79.6	74.5
Open porosity, OP (%)	71.3	68.5	81.9	79.0	80.8	77.6	70.4
Closed porosity, CP (%)	3.1	2.9	0	0.1	0.4	2.0	4.1
Strength determinations							
Compressive strength, σ_{comp} (MPa)			0.33 ± 0.02	0.58 ± 0.14	1.02 ± 0.15	1.39 ± 0.21	2.17 ± 0.13
σ_{bend} (MPa)			20.1	30.5	62.7	75.4	84.1

The actual industrial exploitation of any waste-derived material is limited by the chemical stability. The results of the leaching tests for the best foam from Plasmastone-SLG mixtures, compared to commercial glass foams, are presented in Table 3. In order to assess any impact from the firing temperature, additional foams, with 30 wt% SLG, fired at 800–900 °C, were considered. For all materials, the leaching of Cl, SO_4, Cu, Ni, Ba, Cd, Co, Tl and W are below the limit values for classes U-A (aggregate for unbound or hydraulically or bituminously bound applications with end-of-waste status prior to recycling), U–B (like U–B, but end-of-waste not before recycling) and D (slags) from the Austrian Recycling Construction Materials Ordinance. However, the high quantity of Cr released from Plasmastone-based foams made these materials not suitable for any class. In addition, the released quantities of Mo and V prevented these materials to be classified as D.

Specific SEM microprobe analyses were conducted on foams from Plasmastone-SLG mixtures, in order to understand the origin of the leaching, considering the multiphasic nature of the glass-ceramic materials. Unlike glasses, glass-ceramics do not present a 'homogeneous' chemical behaviour: a significant leaching could be due to high solubility of one heavy metal bearing crystal phase, with a lower soluble residual glass phase, and vice versa.

From Table 4 we can note that the Cr concentration was practically constant in iron silicate-rich zones ('1' in the images of Fig. 5; iron-rich areas were easily detected, due to the light colouration, in backscattered electron images), with increasing firing temperature,

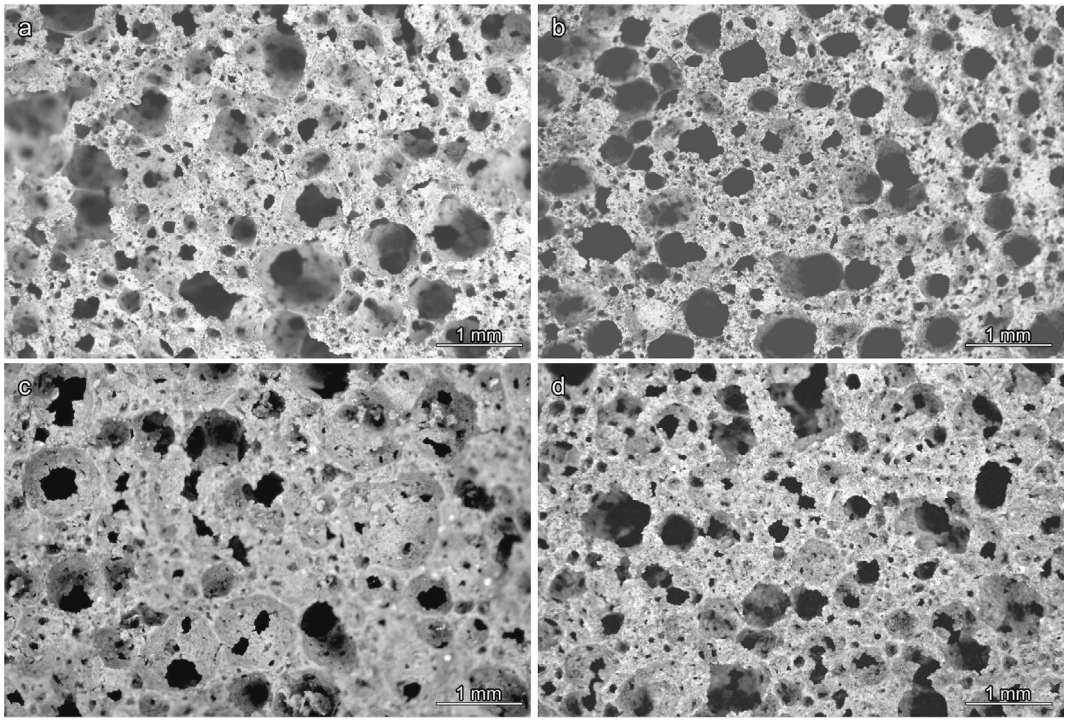

Fig. 4. Micrographs of Plasmastone-derived foams sintered at 1000 °C: a) Pure Plasmastone; b) 10SLG1000; c) 20SLG1000; d) 30SLG1000.

Table 3
Results of the leaching tests on porous materials.

	Reference limits (mg/kg)			*Leaching (mg/kg)*			
	U-A	*U–B*	*D*	Control	70PS800	70PS900	70PS1000
Cr	*0.6*	*1*	*0.3*	0.062	23	18	2.8
Cu	*1*	*2*		0.42	0.022	<0.001	0.067
Ni	*0.4*	*0.6*		0.15	0.0041	0.0033	0.0085
Cl	*800*	*1000*		2.7	2.4	0.94	16
SO_4	*2500*	*6000*		56	38	58	52
Ba			*20*	0.16	0.091	0.23	0.13
Cd			*0.04*	0.017	<0.001	0.0013	0.004
Co			*1*	0.082	0.015	0.013	0.028
Mo			*0.5*	0.072	4.1	5	3.7
Tl			*0.1*	<0.001	0.0041	0.0041	0.0041
V			*1*	0.011	1.5	1.8	1.8
W			*1.5*	0.99	0.79	0.37	0.24
F			*10*	0.55	0.78	0.58	0.76

whereas it decreased in glass/wollastonite zones ('2' in the images of Fig. 5). The reduced leaching of Cr with temperature, especially passing from 900 to 1000 °C, is therefore consistent with the increased crystallization, as shown by Fig. 3c. In particular, Cr could be incorporated in pyroxene (Li et al., 2017). This is again consistent with phase separation in iron-rich glasses; Cr may form Cr-based spinels, having the same crystal structure of magnetite, on which pyroxene crystals grow epitaxially (Goel et al., 2008; Karamanov et al., 2004a).

What envisaged for Cr is not valid for Mo and V. V concentration remained practically unchanged, with firing temperature, in both zones, whereas Mo was 'expelled' from the iron silicate-rich zone.

The chemical stability of the residual glass phase was recognized as the critical point. The precipitation of wollastonite undoubtedly determined an alkali enrichment in the residual glass phase, with consequent reduction of the chemical stability (it is well known that alkali-rich, highly depolymerized glasses are more prone to ionic diffusion) (Bunker, 1994). Mo and V were delicate also for the lacking of additional 'crystal hosts'. If we consider Cu and Ba, nominally concentrated in the glass-wollastonite zone, we could expect a significant release; however, both elements were actually incorporated in Ba-containing copper zinc silicate inclusions, as shown by Fig. 5a (phase labelled with '3').

The suggested use of Plasmastone-based glass-ceramics, as thermally and acoustically insulation materials, should be subjected to some constraints, considering the results of the chemical

Table 4
Microprobe analysis of selected zones of glass-ceramic foams.

	Iron silicate zone			Glass/wollastonite zone		
Firing T (°C)	800	900	1000	800	900	1000
Metal concentration (%)						
Mo	0.0310	0.0081	0.0060	0.0117	0.0081	0.0091
Fe	15.47	15.70	15.20	1.88	2.57	3.81
Cu	0.0033	0.0119	0.0514	0.0990	0.0826	0.0519
Ba	0.0015	0.0081	0.0033	0.0177	0.0241	0.0217
Zn	0.0022	0.0005	0.0014	0.0067	0.0138	0.0017
V	0.0367	0.0358	0.0394	0.0066	0.0091	0.0089
Cr	0.0102	0.0125	0.0123	0.0269	0.0159	0.0094

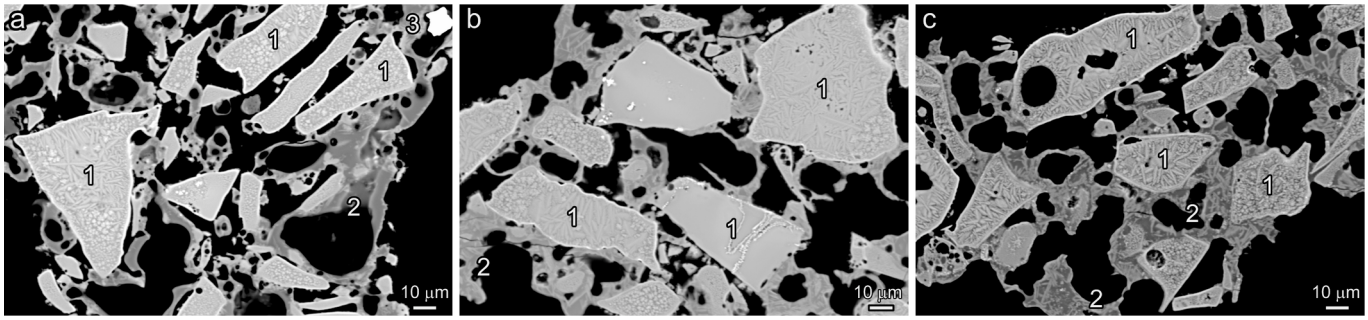

Fig. 5. Micrographs of porous Plasmastone/30% soda-lime glass materials: a) 800 °C; b) 900 °C; c) 1000 °C [1: iron silicate zone; 2: glass/wollastonite zone; 3: inclusion].

analyses and leaching tests. Above all, only foams sintered at 1000 °C could be considered. In addition, the foams could only be applied in dry conditions or embedded in a more chemically stable matrix. A possible suggestion concerns the cladding with a geopolymeric paste, thus configuring sandwich structures, exploiting the easy low temperature processing and the high chemical stability of geopolymers (Lancellotti et al., 2010).

'A priori' modifications of Plasmastone, i.e. a revision of the overall formulation, could be a further possibility. It should be noted that the plasma processing conditions could be adjusted in order to enhance the separation of metals, that could include also the environmentally relevant elements, such as Cr, Mo and V. This enhancement would increase also the overall amounts of SiO_2 and Al_2O_3 in the vitreous residue. In any case, 'a posteriori' modifications were still applied. A boro-alumino-silicate glass (BSG), from pharmaceutical vials, was finally used instead of common soda-lime glass, mixed with Plasmastone in an amount of 30 wt%. A 'zero waste' approach was saved, since discarded or end-of-use pharmaceutical vials constitute a specific kind of waste, being excluded from direct recycling in the manufacturing of new vials (Ponsot et al., 2014).

The change of glass additive implied longer low temperature hardening steps, as an effect of the reduced CaO content of BSG. The adopted gel casting approach, in any case, led to quite homogeneous cellular structures, well maintained after firing at 1000 °C, as shown by Fig. 6.

The change in the glass further modified the phase assemblage. From Fig. 3c we can observe that with the second glass additive the firing at 1000 °C led to glass-ceramics with only hedenbergite and andradite. The latter decreased passing from pure Plasmastone to soda-lime glass containing mixtures: the boro-alumino-silicate glass favoured its recovery. We can also note an increase in the amorphous background, consistent with the shiny glassy appearance of cell walls in Fig. 6. The new phase assemblage was advantageous for the mechanical properties, as shown by Table 2, with improvements in both compressive strength and strength of the solid phase.

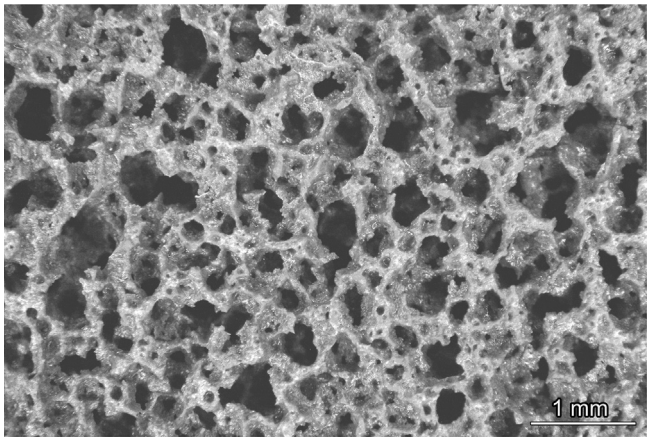

Fig. 6. Microstructural details of BSG-modified Plasmastone-based foams.

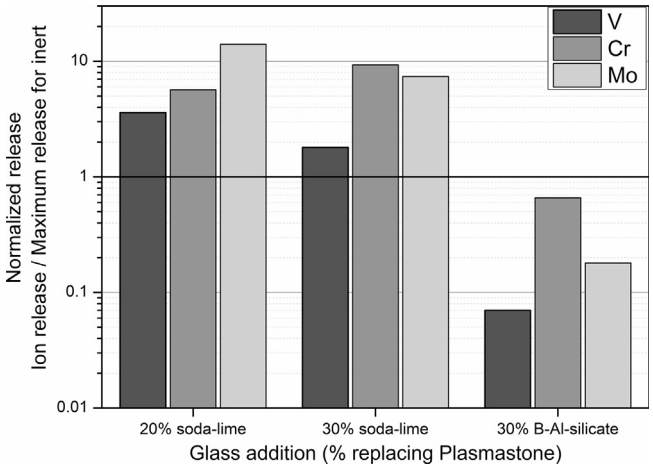

Fig. 7. Leaching results of Cr, Mo and V normalized by the Class D of the Austrian Regulation limits.

The leaching tests indicated a very good stabilization of any pollutant. Fig. 7, in particular, shows the releases of the critical pollutants (Cr, Mo and V), normalized by class D thresholds of the Austrian regulation, of the last foams (with 30% boro-alumino-silicate glass) compared with those from soda-lime glass (20% or 30%). There was a spectacular reduction of more than one order of magnitude in the overall releases of critical elements. The other elements (not shown for the sake of brevity), already below the thresholds for soda-lime glass, were maintained below the limits. In other words, the foams from the use of pharmaceutical glass could be considered as perfectly 'safe'.

4. Conclusions

We may conclude that:

- Highly porous Plasmastone/waste glass glass-ceramics (porosity exceeding 75 vol%) were successfully obtained by the combined technique of alkali activation, gel-casting and sintering.
- Waste glass additions increased the gelification and also the strength of the solid phase.

- The enhancement of sintering temperature, and consequently of crystallization, helped in reducing the leaching of hazardous elements, with some exceptions (Cr, Mo, V).
- The use of boro-alumino-silicate glass, instead of common soda-lime glass, decreased also the leaching of Cr, Mo and V underneath the limit values for slag-derived construction materials in Austria, maintaining high porosity and good mechanical properties.

'Declarations of interest: none'.

Acknowledgement

The research leading to these results has received funding from the European Union's Horizon 2020 research and innovation programme under the Marie Sklodowska-Curie grant agreements No. 721185 “NEW-MINE” (EU Training Network for Resource Recovery through Enhanced Landfill Mining - Patricia Rabelo Monich, Daniel Höllen and Enrico Bernardo) and No. 642557 “CoACH-ETN” (Advanced glasses, Composites And Ceramics for High growth Industries European Training Network - Acacio Rincón Romero and Enrico Bernardo).

References

Bernardo, E., Scarinci, G., Maddalena, A., Hreglich, S., 2004. Development and mechanical properties of metal-particulate glass matrix composites from recycled glasses. Compos. Part A Appl. Sci. Manuf 35, 17–22. https://doi.org/10.1016/j.compositesa.2003.09.022.

Bernardo, E., Bonomo, E., Dattoli, A., 2010. Optimisation of sintered glass – ceramics from an industrial waste glass. Ceram. Int. 36, 1675–1680. https://doi.org/10.1016/j.ceramint.2010.02.047.

Bunker, B.C., 1994. Molecular mechanisms for corrosion of silica and silicate glasses. J. Non-Cryst. Solids 179, 300–308. https://doi.org/10.1016/0022-3093(94)90708-0.

Cyr, M., Idir, R., Poinot, T., 2012. Properties of inorganic polymer (geopolymer) mortars made of glass cullet. J. Mater. Sci. 47, 2782–2797. https://doi.org/10.1007/s10853-011-6107-2.

Elsayed, H., Romero, A.R., Ferroni, L., Gardin, C., Zavan, B., Bernardo, E., 2017. Bioactive glass-ceramic scaffolds from novel “inorganic gel casting” and sinter-crystallization. Materials 10. https://doi.org/10.3390/ma10020171.

Garcia-Lodeiro, I., Aparicio-Rebollo, E., Fernández-Jimenez, A., Palomo, A., 2016. Effect of calcium on the alkaline activation of aluminosilicate glass. Ceram. Int. 42, 7697–7707. https://doi.org/10.1016/j.ceramint.2016.01.184.

Gibson, L.J., Ashby, M.F., 1999. Cellular Solids: Structure and Properties. Cambridge University Press, Cambridge, UK.

Goel, A., Tulyaganov, D.U., Kharton, V.V., Yaremchenko, A.A., Ferreira, J.M.F., 2008. The effect of Cr_2O_3 addition on crystallization and properties of La_2O_3-containing diopside glass-ceramics. Acta Mater. 56, 3065–3076. https://doi.org/10.1016/j.actamat.2008.02.036.

Höland, W., Beall, G.H., 2002. Glass Ceramic Technology. The American Ceramic Society, Ohio.

Jones, P.T., Geysen, D., Tielemans, Y., Van Passel, S., Pontikes, Y., Blanpain, B., Quaghebeur, M., Hoekstra, N., 2013. Enhanced Landfill Mining in view of multiple resource recovery: a critical review. J. Clean. Prod. 55, 45–55. https://doi.org/10.1016/j.jclepro.2012.05.021.

Karamanov, A., Pisciella, P., Cantalini, C., Pelino, M., 2000. Influence of Fe^{3+}/Fe^{2+} ratio on the crystallisation of Iron-rich glasses made with industrial wastes. J. Th 83, 3153–3157. https://doi.org/10.1111/j.1151-2916.2000.tb01697.x.

Karamanov, A., Arrizza, L., Matekovits, I., Pelino, M., 2004a. Properties of sintered glass-ceramics in the diopside-albite system. Ceram. Int. 30, 2129–2135. https://doi.org/10.1016/j.ceramint.2003.11.019.

Karamanov, A., Taglieri, G., Pelino, M., 2004b. Iron-rich sintered glass-ceramics from industrial wastes. J. Am. Ceram. Soc. 82, 3012–3016. https://doi.org/10.1111/j.1151-2916.1999.tb02195.x.

Krook, J., Svensson, N., Eklund, M., 2012. Landfill mining: a critical review of two decades of research. Waste Manag. 32, 513–520. https://doi.org/10.1016/j.wasman.2011.10.015.

Lancellotti, I., Kamseu, E., Michelazzi, M., Barbieri, L., Corradi, A., Leonelli, C., 2010. Chemical stability of geopolymers containing municipal solid waste incinerator fly ash. Waste Manag. 30, 673–679. https://doi.org/10.1016/j.wasman.2009.09.032.

Li, J., Liu, B., Zeng, Y., Wang, Z., 2017. Mineralogical determination and geo-chemical modeling of chromium release from AOD slag: distribution and leachability aspects. Chemosphere 167, 360–366. https://doi.org/10.1016/j.chemosphere.2016.10.020.

Machiels, L., Arnout, L., Yan, P., Jones, P.T., Blanpain, B., Pontikes, Y., 2016. Transforming enhanced landfill mining derived gasification/vitrification glass into low-carbon inorganic polymer binders and building products. J. Sustain. Metall. 1–11. https://doi.org/10.1007/s40831-016-0105-1.

Mastelaro, V.R., Zanotto, E.D., 1996. Residual stresses in a soda-lime-silica glass-ceramic. J. Non-Cryst. Solids 194, 297–304. https://doi.org/10.1016/0022-3093(95)00509-9.

Misapor, 2017. Misapor [WWW Document]. http://www.misapor.ch/EN/Home.html (Accessed November 2017).

Norm EN 12457–4, 2002. Norm EN 12457–4.

Pisciella, P., Pelino, M., 2005. FTIR spectroscopy investigation of the crystallisation process in an iron rich glass. J. Eur. Ceram. Soc. 25, 1855–1861. https://doi.org/10.1016/j.jeurceramsoc.2004.06.012.

Ponsot, I.M.M.M., Pontikes, Y., Baldi, G., Chinnam, R.K., Detsch, R., Boccaccini, A.R., Bernardo, E., 2014. Magnetic glass ceramics by sintering of borosilicate glass and inorganic waste. Materials 7, 5565–5580. https://doi.org/10.3390/ma7085565.

Rincón, A., Marangoni, M., Cetin, S., Bernardo, E., 2016. Recycling of inorganic waste in monolithic and cellular glass-based materials for structural and functional applications. J. Chem. Technol. Biotechnol. 91, 1946–1961. https://doi.org/10.1002/jctb.4982.

Rincón, A., Giacomello, G., Pasetto, M., Bernardo, E., 2017. Novel “inorganic gel casting” process for the manufacturing of glass foams. J. Eur. Ceram. Soc. 37, 2227–2234. https://doi.org/10.1016/j.jeurceramsoc.2017.01.012.

Scanarc, 2017. Scanarc [WWW Document]. http://www.scanarc.se/ (Accessed November 2017).

Strozi Cilla, M., Colombo, P., Raymundo Morelli, M., 2014. Geopolymer foams by gelcasting. Ceram. Int. 40, 5723–5730. https://doi.org/10.1016/j.ceramint.2013.11.011.

Winterstetter, A., Laner, D., Rechberger, H., Fellner, J., 2015. Framework for the evaluat of anthropogenic resources: a landfill mining case study - resource or reserve? Resour. Conserv. Recycl. 96, 19–30. https://doi.org/10.1016/j.resconrec.2015.01.004.

Wolfsberger, T., Aldrian, A., Sarc, R., Hermann, R., Höllen, D., Budischowsky, A., Zöscher, A., Ragoßnig, A., Pomberger, R., 2015a. Landfill mining: resource potential of Austrian landfills – evaluation and quality assessment of recovered municipal solid waste by chemical analyses. Waste Manag. Res. 33, 962–974. https://doi.org/10.1177/0734242X15600051.

Wolfsberger, T., Nispel, J., Sarc, R., Aldrian, A., Hermann, R., Höllen, D., Pomberger, R., Budischowsky, A., Ragossnig, A., 2015b. Landfill mining: development of a theoretical method for a preliminary estimate of the raw material potential of landfill sites. Waste Manag. Res. 33, 671–680. https://doi.org/10.1177/0734242X15590473.